

Contents lists available at ScienceDirect

Computers & Fluids

journal homepage: www.elsevier.com/locate/compfluid



Nonuniform-time-step explicit Runge-Kutta scheme for high-order finite difference method



Li Liu a,c, Xiaodong Li a,*, Fang Q. Hu b

- ^a School of Energy and Power Engineering, Beihang University, Beijing 100191, People's Republic of China
- ^b Department of Mathematics and Statistics, Old Dominion University, Norfolk, Virginia 23529, United States
- ^c Beijing Institute of Space Launch Technology, Beijing 100076, People's Republic of China

ARTICLE INFO

Article history: Received 2 October 2013 Received in revised form 12 March 2014 Accepted 3 September 2014 Available online 16 September 2014

Keywords: Explicit Runge-Kutta method High order finite difference method Computational aeroacoustics

ABSTRACT

Explicit Runge–Kutta method has been widely used for time-accurate simulations in aeroacoustics and aerodynamics, partly because of its strong stability properties. However, when dealing with problems involving irregular geometries or multi-scale phenomena where the grid is often refined in localized regions, a single global time step size dictated by the smallest grid size based on the explicit stability condition would inevitably result in excessive computational consumption. A local time stepping strategy that adopts time step size to the local stability requirement in different grid blocks is an effective way to reduce the cost of time integration and to increase the overall computational efficiency. In the present paper, a non-uniform time step (NUTS) explicit Runge–Kutta scheme, previously introduced in the framework of discontinuous Galerkin method, which makes the local time stepping strategy applicable to the explicit Runge–Kutta family without any interpolation and extrapolation in time, is further extended to high-order finite difference methods. The stability of non-uniform time step (NUTS) scheme in combination with high order difference schemes is studied. Numerical experiments are carried out using 1D and 2D acoustic problems for validation of the proposed approach. Computational cost reduction by the proposed algorithm is also discussed.

© 2014 Elsevier Ltd. All rights reserved.

1. Introduction

A wide range of aeroacoustic problems concern with the noise phenomena produced by interactions between the unsteady flows and embedded solid bodies, including the generation of aerodynamic sound and its propagation in a large acoustic field. Due to the great differences in the length scale as well as the magnitude of the fluid flows and acoustic disturbances, accurate prediction of these phenomena requires spatial and temporal algorithms of low dissipation and low dispersion errors [1]. In the past few decades, optimized high-order finite difference schemes and highorder time integration have been developed in computational aeroacoustics (CAA) [1-4,20-22], and shown to be reliable in a variety of aeroacoustic applications. The development of overset grid techniques [5,8,6,7] based on high-order interpolation and extrapolation technique [11,9,10] has made finite difference schemes capable of dealing with complex problems involving irregular geometries, where the grids are refined in the immediate vicinities of the solid body to accurately capture aerodynamic structures and coarsened in the region far away from the solid boundaries that would be adequate to resolve the acoustic scale. However, computational efficiency of high-order explicit time integration with a single uniform time-step size dictated by the smallest grid size based on the stability requirement can lead to excessive computational cost in the application of finite difference techniques to many practical complex problems in computational aeroacoustics.

Local time stepping strategy that uses local time-step size for time marching is one of the effective ways to reduce the overall computational time for temporal integration, and has attracted much attentions recently [12,13,16,14,15,17,18]. Some of these works are based on the multi-step time integration schemes, such as Adams-Bashforth method, or employ the high-order optimized interpolation technique for communications between different time levels. For high-order explicit Runge-Kutta integration methods (RK), which is popular time integration schemes in aero-dynamic and aeroacoustic simulations, multirate algorithms has been introduced for solving the stiff system with the aid of interpolation and the extrapolation in time [15,18]. Recently, a high-order coupling procedure without interpolation and extrapolation in time, called non-uniform-time-step explicit Runge-Kutta scheme

^{*} Corresponding author. E-mail address: lixd@buaa.edu.cn (X. Li).

$ar{v}$ mean velocity in the y direction $ar{p}$ mean pressure $ar{a}$ mean velocity of sound M_x Mach number in the x direction M_y Mach number in the y direction	$\mathbf{U}^{(i)}, \mathbf{k}_i$ \mathbf{R} λ CFL S, S^*	stage values of RK integration amplification matrix eigenvalue of amplification matrix Courant-Friedrichs-Lewy number time cost reduction factor	
-------------------------------------------------------------------------------------------------------------------------------------------------------------------------	------------------------------------------------------------------------	--------------------------------------------------------------------------------------------------------------------------------------------------------------	--

(NUTS-RK) [19], has been developed, making the local time stepping strategy available for explicit Runge–Kutta methods. In Ref. [19], linear formulation of the scheme has been proposed for various explicit RK schemes that are used frequently in CAA, and has been demonstrated in the framework of discontinuous Galerkin (DG) finite element method.

In the present paper, we will further explore the application of NUTS-RK to typical high-order spatial difference discretization in CAA, for example, the dispersion-relation-preserving (DRP) finite difference scheme [1], and discuss some implementational issues of this application on overlapping grids for aeroacoustic computations. The numerical algorithm involved is first reviewed in Section 2. In Section 3, the stability of NUTS-RK applied to high-order finite difference schemes is examined in one space dimension. Section 4 gives the numerical validations carried out in one and two dimensional examples. Finally, Section 5 includes the conclusions.

2. Nonuniform-time-step explicit Runge-Kutta method

The general linear formulation of non-uniform time step Runge–Kutta scheme, given in Ref. [19], is reviewed briefly at first. After a spatial discretization by finite difference scheme, the semi-discretized equation to be advanced in time can be modeled as follows

$$\frac{\partial \mathbf{U}}{\partial t} = F(\mathbf{U}) \tag{1}$$

where **U** denotes the solution at the grid points. A general *p*-stage explicit Runge–Kutta integration for advancing solution from $t = t_n$ to $t = t_n + \Delta t$ can be expressed as follows,

$$\begin{aligned} & \mathbf{k}_{1} = F(\mathbf{U}^{n}), \mathbf{U}^{(1)} = \mathbf{U}^{n} + \Delta t a_{21} \mathbf{k}_{1} \\ & \mathbf{k}_{2} = F(\mathbf{U}^{(1)}), \mathbf{U}^{(2)} = \mathbf{U}^{n} + \Delta t (a_{31} \mathbf{k}_{1} + a_{32} \mathbf{k}_{2}) \\ & \cdots \\ & \mathbf{k}_{p-1} = F(\mathbf{U}^{(p-2)}), \mathbf{U}^{(p-1)} = \mathbf{U}^{(0)} + \Delta t [a_{p1} \mathbf{k}_{1} + a_{p2} \mathbf{k}_{2} + \cdots + a_{pp-1} \mathbf{k}_{p-1}] \\ & \mathbf{k}_{p} = F(\mathbf{U}^{(p-1)}) \\ & \mathbf{U}^{n+1} = \mathbf{U}^{n} + \Delta t \sum_{i=1}^{p} b_{i} \mathbf{k}_{i} \end{aligned}$$

$$(2)$$

where \mathbf{U}^n and \mathbf{U}^{n+1} indicate the numerical solutions at time level t_n and $t_{n+1} = t_n + \Delta t$, respectively. Here, $\mathbf{U}^{(i)}$ and \mathbf{k}_i are the stage values for the RK integration.

The exact linear relation between k_i and time derivatives $\frac{\partial^0 \mathbf{U}}{\partial t^0}$ can be found as [19,20]

where the entries of matrix \mathbf{C} are constants and related to the RK coefficients a_{ij} and given in detail in Ref. [19]. This relation allows the coupling of solutions between blocks employing different local time steps without interpolation and extrapolation in time.

Now consider the coupling formulas for time stepping in a finite difference scheme, in two blocks next to each other and with different time step sizes, denoted as Mesh 1 with Δt_1 and Mesh 2 with Δt_2 in Fig. 1.

For time stepping in Mesh 1, to advance solution from t_n to t_{n+1} , using the relation given in (3), the required stage values at $t = t_n$ on grid points inside block 2 can be obtained as

$$[\widetilde{\mathbf{K}}_2]_{t=t_n} = \mathbf{C}\mathbf{P}_{\Delta t_1}\mathbf{B}_{\Delta \tau_2}\mathbf{P}_{\Delta t_2}^{-1}\mathbf{C}^{-1}[\mathbf{K}_2]_{t=t_{m-1}} \tag{4}$$

where $t_{m-1} < t_n$ and $\Delta \tau_2 = t_n - t_{m-1}$. Here, a tilde is used to indicate the **k** values to be used in the neighboring block. Likewise, for time stepping in Mesh 2, to advance solution from t_m to t_{m+1} , the required stage values on the grid points inside block 1 are computed by

$$[\widetilde{\mathbf{K}}_1]_{t=t_m} = \mathbf{C}\mathbf{P}_{\Delta t_2}\mathbf{B}_{\Delta \tau_1}\mathbf{P}_{\Delta t_1}^{-1}\mathbf{C}^{-1}[\mathbf{K}_1]_{t=t_n}$$

$$\tag{5}$$

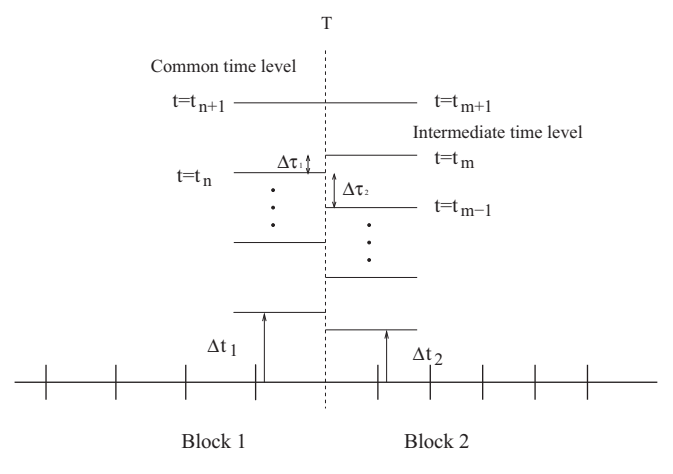


Fig. 1. Schematics of nonuniform time-step advancing in a nonuniform grid.

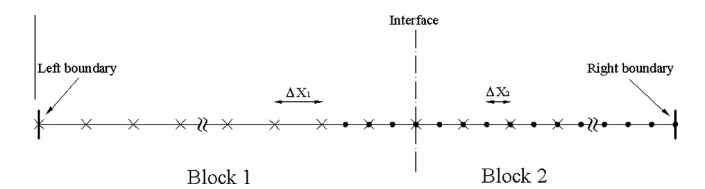


Fig. 2. Schematic of a 1D overset grid for finite difference discretization.

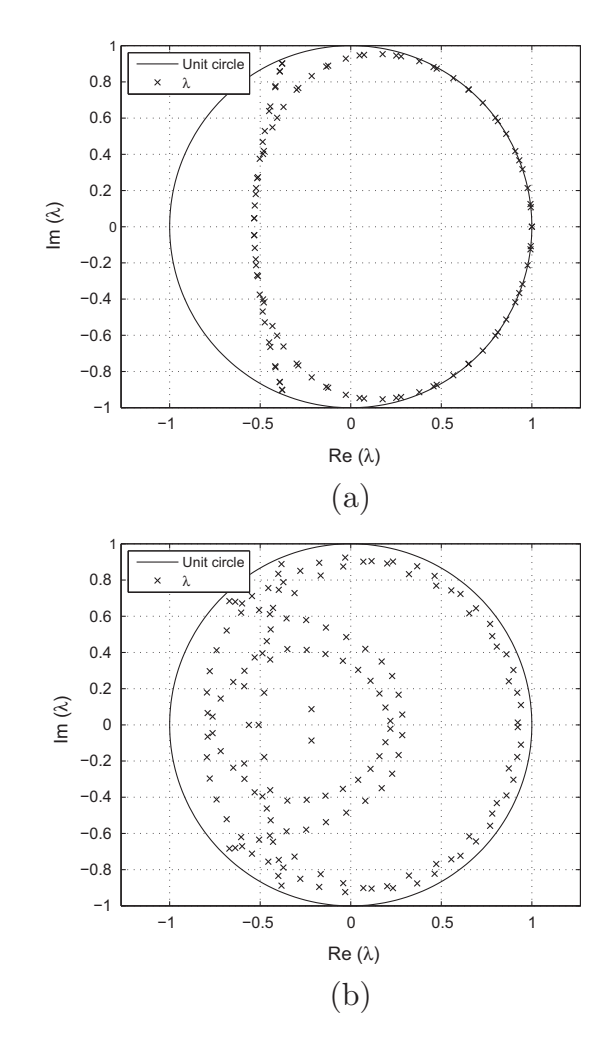
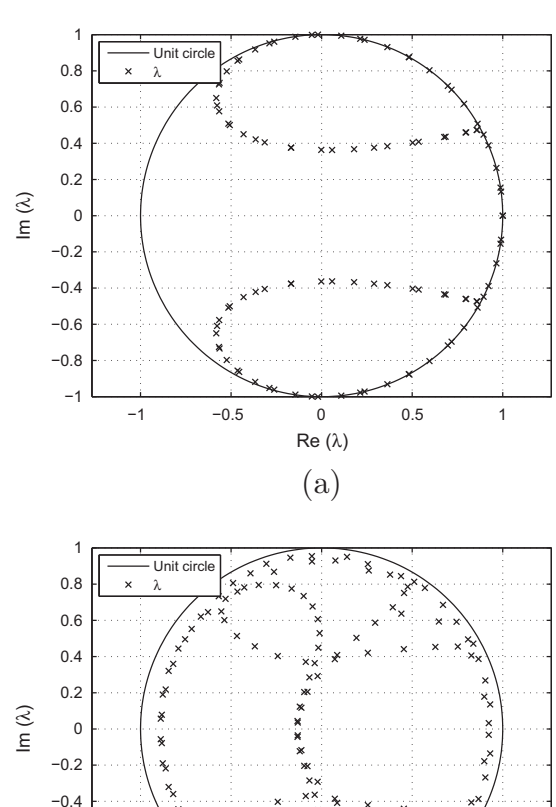


Fig. 3. Distribution of eigenvalues of the amplification matrix R for LDDRK4-DRP: (a) uniform time step when $\mbox{\it CFL}=1.73$ and (b) non-uniform time step when CFL = 1.73.

where $t_n < t_m$ and $\Delta \tau_1 = t_m - t_n$. Matrix $\mathbf{B}_{\Delta \tau}$ appeared in (4) and (5) is derived from Taylor series expansion of vector $[\mathbf{K}]$, and the details can be found in Appendix A.

In practice, the coupling procedures formulated by (4) and (5) can result in two cases, of which one is synchronous stepping and the other is nonsynchronous stepping. When the neighboring grid blocks are to advance from the same time level, i.e., when t_n coincides with t_m , the coupled integration at the overset grids between those blocks should be executed synchronously by formula (4) and (5), where $\Delta \tau = 0$ and $\mathbf{B}_{\Delta \tau}$ is an identity matrix. That means the coupling procedures should be carried out at each stage of RK integration. When the neighboring grid blocks is to advance from different time levels, i.e., when t_n is different from t_m , the coupled integration described by (4) and (5) needs be executed individually on the block, which is referred to as nonsynchronous stepping.



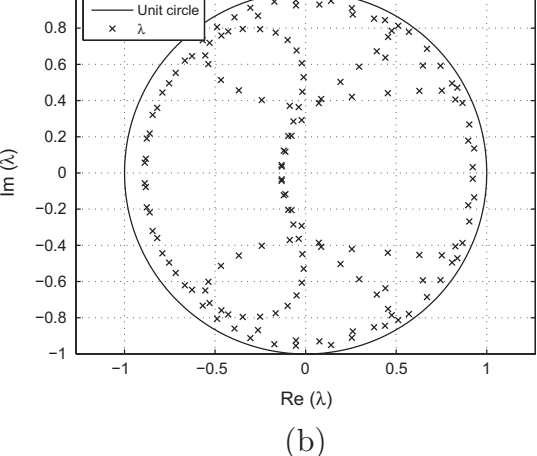


Fig. 4. Distribution of eigenvalues of the amplification matrix R for LDDRK5- $DRP(\mathcal{O}(4))$: (a) uniform time step when CFL=2.14 and (b) non-uniform time step when CFL = 2.14.

Table 1 Stability limits of 1D LDDRK-DRP.

Stage of LDDRK	Non-uniform time step		Uniform time step	
	CFL (by (9))	CFL (numerical)	CFL (by (9))	CFL (numerical)
4	1.73	1.74	1.73	1.73
5	2.14	2.14	2.14	2.14
6	1.00	1.01	1.00	1.04

Note: In non-uniform time step, $\Delta t_1 : \Delta t_2 = \Delta x_1 : \Delta x_2 = 2 : 1$.

When the intermediate stage values are computed by (4) and (5), no interpolation or extrapolation is necessary.

Once the coupled stage values $\tilde{\mathbf{k}}_i$ are obtained by (4) and (5), the coupled values $\widetilde{\mathbf{U}}^{(j)}$ can be computed according to formula (2). With finite difference discretization on overset grids, only the coupled values $\tilde{\mathbf{U}}^{(j)}$ that are to be interchanged between neighboring blocks are needed at each stage. That means the coupling procedures for non-uniform time step RK integration are only executed on a small number of grid points for spatial interpolation and not on the entire grid of the computational domain.

3. Stability analysis

In this section, the stability property of the above non-uniform time step explicit Runge-Kutta scheme combined with a

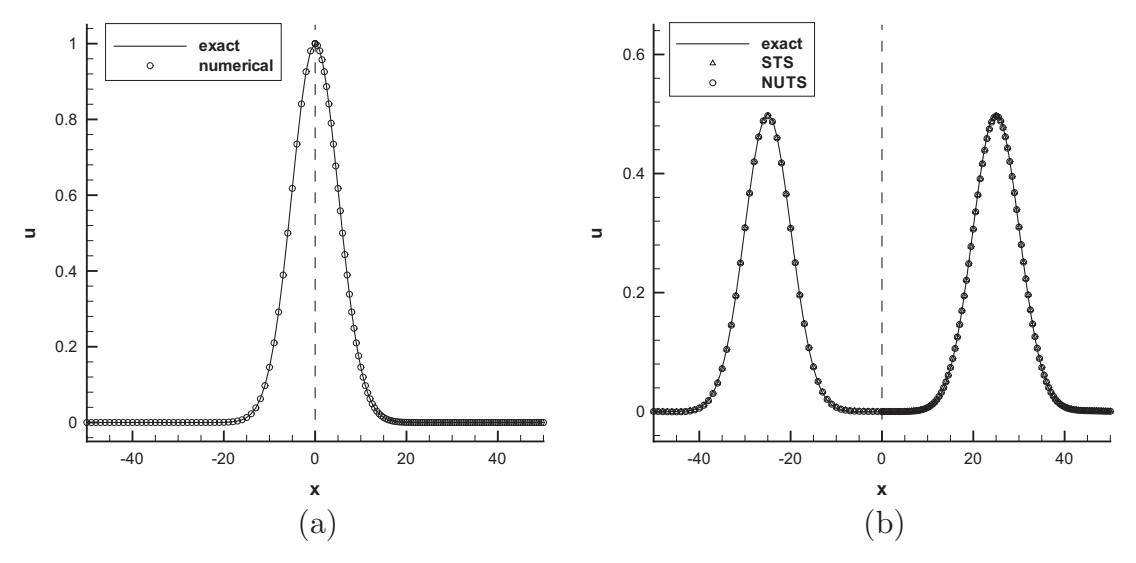


Fig. 5. The solution in 1D overset grid: (a) t = 0 and (b) t = 625.

Table 2
The cost reductions by NUTS-RK for cases presented in Section IV.

Examples	Case A	Case B.1	Case B.2	
			$AOA = 0^{\circ}$	$AOA = 2^{\circ}$
S(%)	73.8	82.3	74.3	77.4
S *(%)	72.4	75.8	71.6	74.4

high-order finite difference discretization will be investigated. A one-dimensional convective equation will be used as the model equation for our analysis, as follows:

$$\frac{\partial u}{\partial t} + a \frac{\partial u}{\partial x} = 0 \tag{6}$$

The spatial discretization is done by a central difference scheme in a one dimensional overlapping grid depicted in Fig. 2. The 7-point DRP scheme will be used as an example. The non-uniform grid consists of two blocks, and both are in turn partitioned uniformly by

104 grid points within the block. For each block, 3 points are located at the other side of the interface between the blocks. As an example, the spacings of grid points in two blocks satisfy $\Delta x_1 : \Delta x_2 = 2 : 1$.

Since a 7-point stencil is used in spatial discretization, the values at the last 3 points of each block in the overlapping area that are not immediately available have to be found by spatial interpolation for data transfer between the overlapping blocks. Here the interpolation algorithm suggested in Ref. [11] is adopted. The periodic boundary condition is assumed at the left and the right of the computational domain as indicated in Fig. 2. The finite difference semi-discretization of (6) as described above can be written in a global-matrix form as follows:

$$\frac{\partial \mathbf{U}}{\partial t} = \mathbf{H}\overline{\mathbf{U}} \tag{7}$$

where $\overline{\mathbf{U}}$ is a column vector containing all solutions at grid points. \mathbf{H} is a constant matrix that depends on the specific finite difference scheme and the spatial interpolation formula.

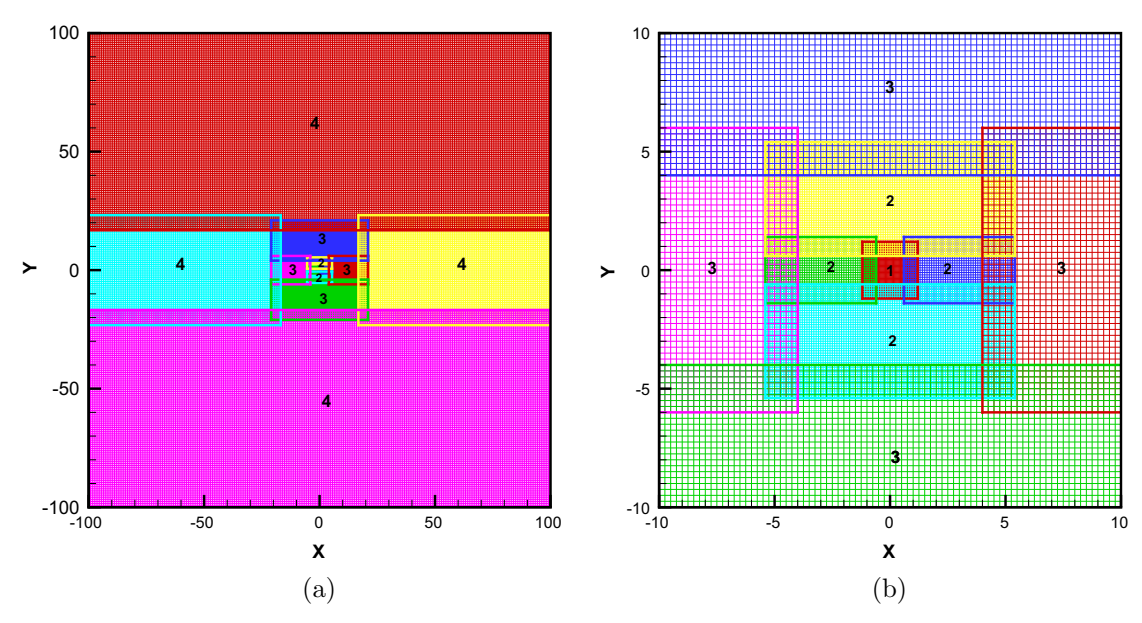


Fig. 6. 2D overset grid: (a) whole and (b) local.

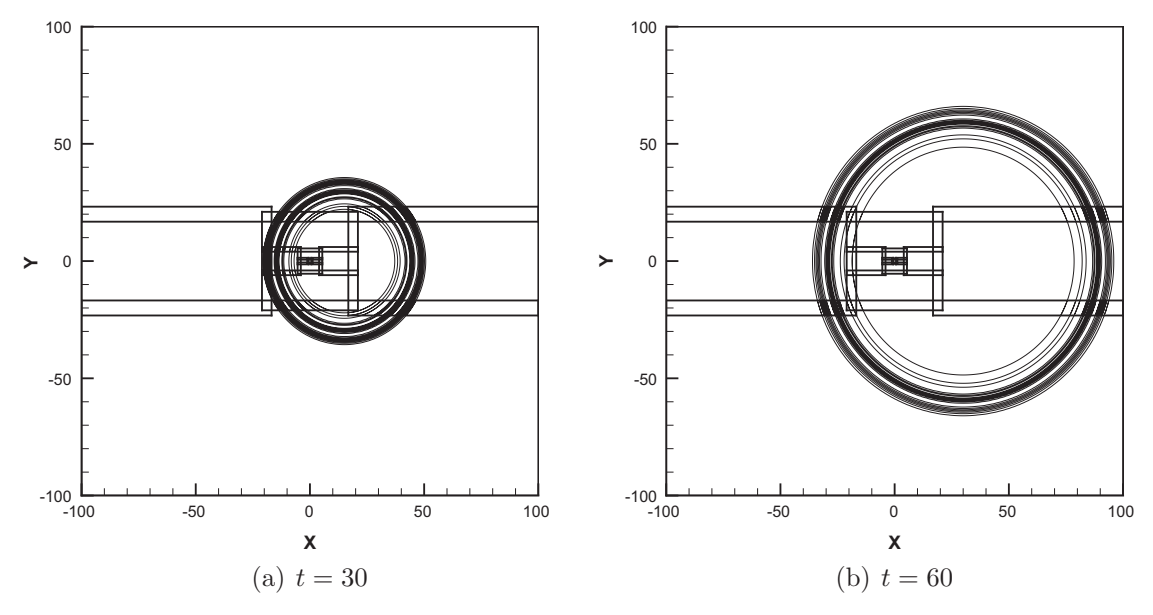


Fig. 7. Contours of pressure with $M_x = 0.5$, and $M_y = 0$.

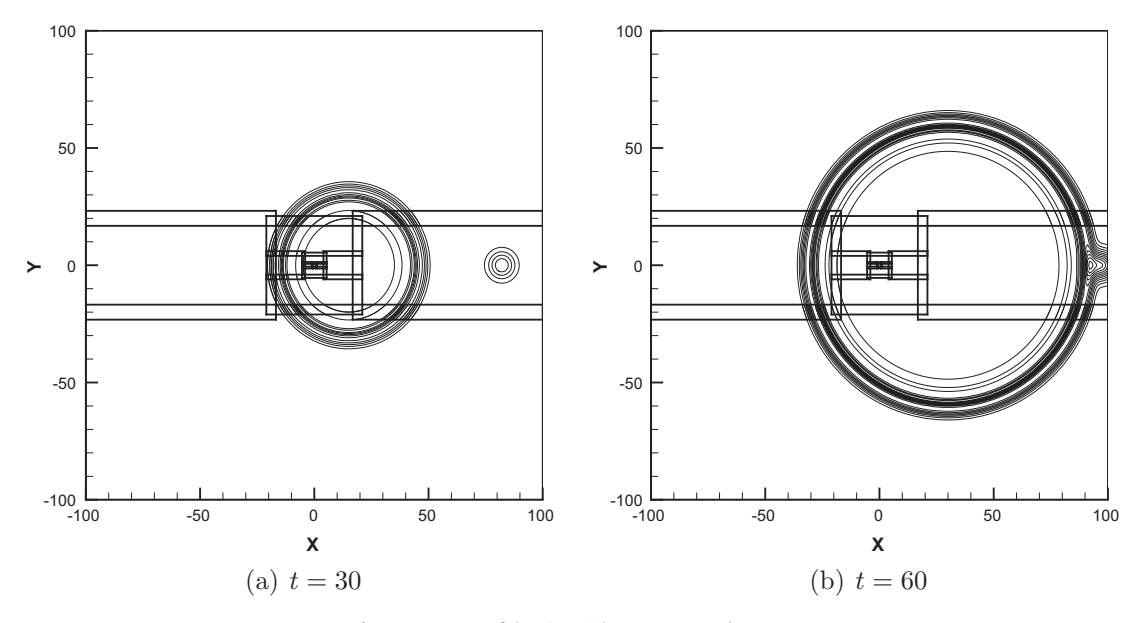


Fig. 8. Contours of density with $M_x = 0.5$, and $M_y = 0$.

We assume that a uniform CFL number is used in the whole domain, which leads to time step sizes of two blocks in the current example as $\Delta t_1: \Delta t_2=2:1$. By applying the explicit RK integration with non-uniform time steps described in Section 2 to Eq. (7), it is straightforward to find the amplification matrix **R** that gives

$$\overline{\mathbf{U}}^{n+1} = \mathbf{R}\overline{\mathbf{U}}^n \tag{8}$$

Then the stability of the scheme can be investigated by checking if the modulus of eigenvalues of ${\bf R}$ satisfy the condition expressed as

$$\max(|\lambda_i|) \leqslant 1 \tag{9}$$

where λ_i are the eigenvalues of **R**.

The distribution of eigenvalues of the amplification matrix **R** for the non-uniform time step (NUTS) low-dissipation and low-dispersion Runge–Kutta methods (LDDRK) [20], with DRP spatial difference scheme, has been computed for this example. Distribu-

tion of eigenvalues is shown in Figs. 3 and 4 for LDDRK4 (4 stages) and LDDRK5 (5 stages) respectively. The stability limits obtained analytically by (9) are also compared with the ones found by direct numerical simulation of the 1D problem and shown in Table 1. The comparison shows that the stability limits on local CFL number for non-uniform time steps are almost identical to those for a single uniform time step, which means the coupling procedures for non-uniform time-step size preserve the original stability limits of the LDDRK schemes well.

4. Numerical validation

4.1. One dimensional case

The present algorithm is first validated for a one-dimensional two-way wave equation, which is described by the equation and initial condition listed below,

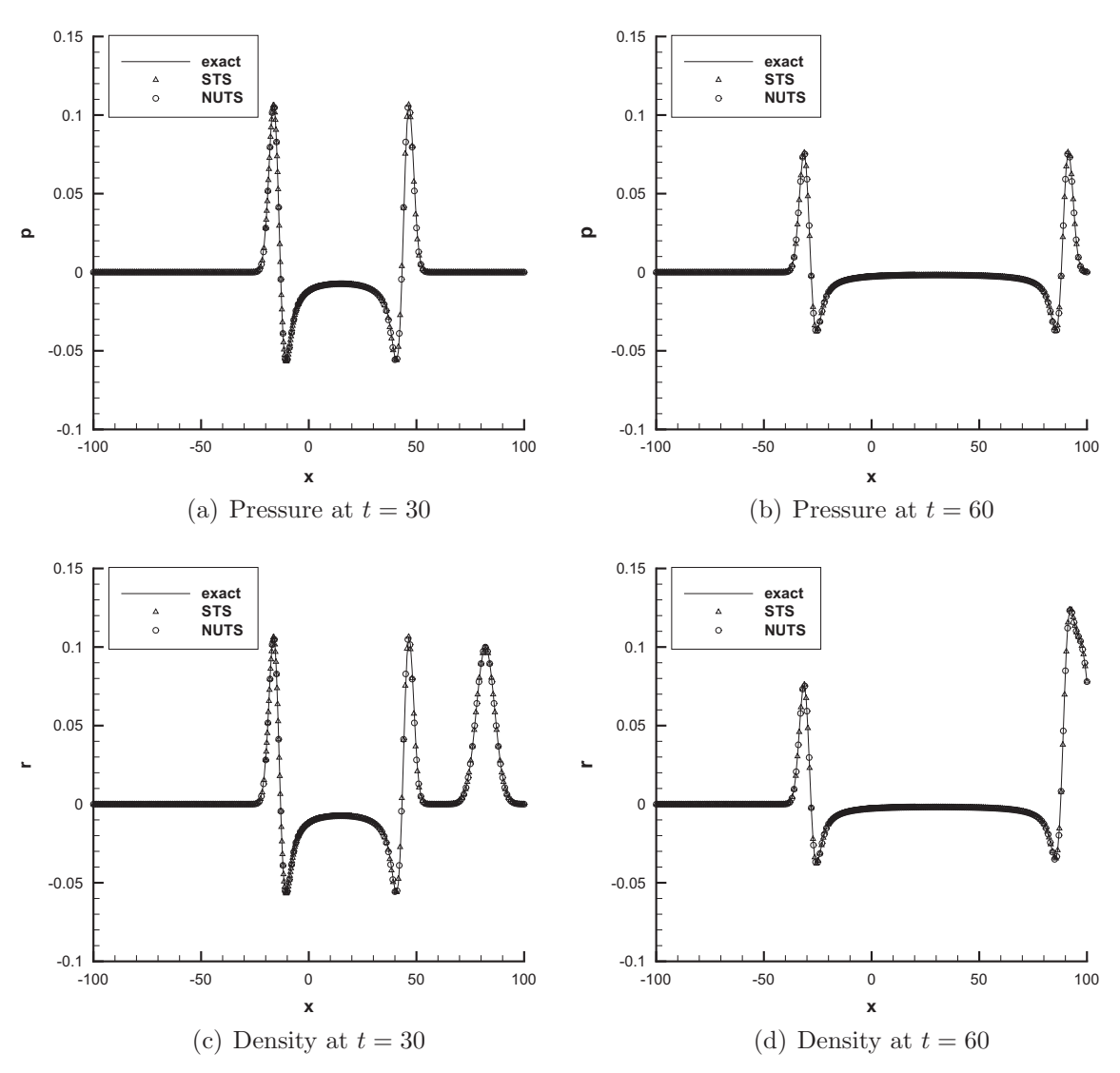


Fig. 9. Comparison of numerical and exact solutions along the line y = 0 with $M_x = 0.5$, and $M_y = 0$.

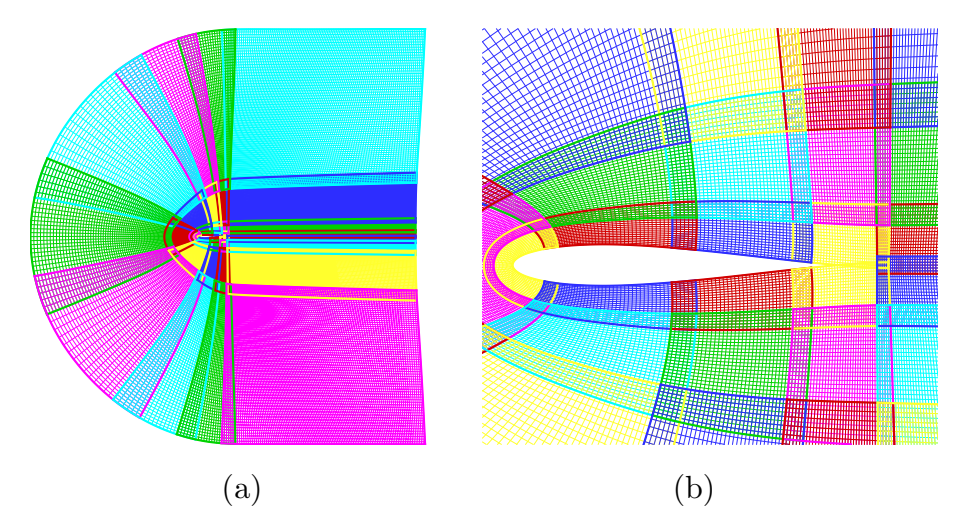


Fig. 10. The body-fitted overset grid around airfoil: (a) whole and (b) local.

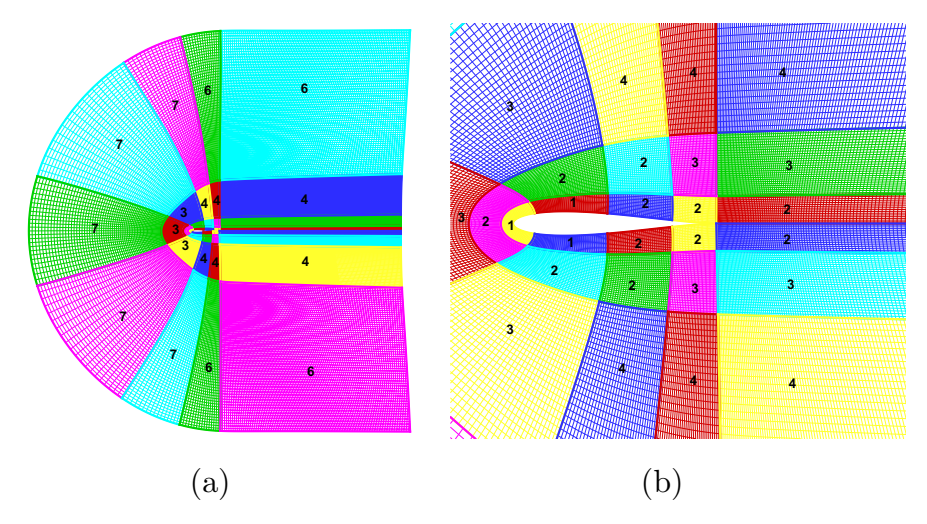


Fig. 11. Distribution of the time-step sizes: (a) whole and (b) local.

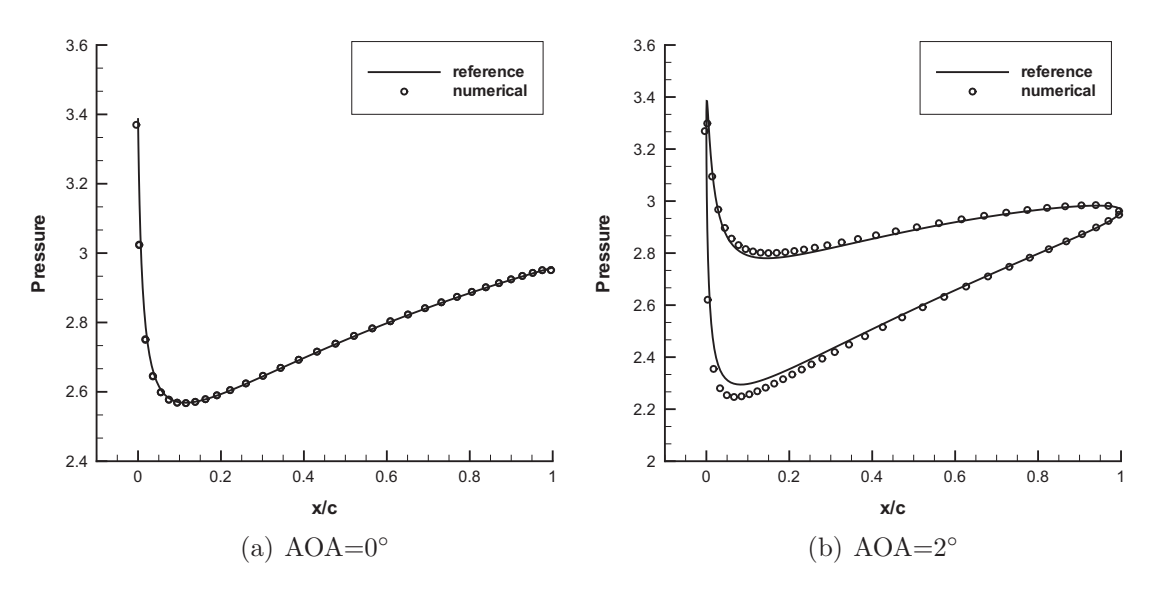


Fig. 12. Mean pressure distribution on the airfoil surface.

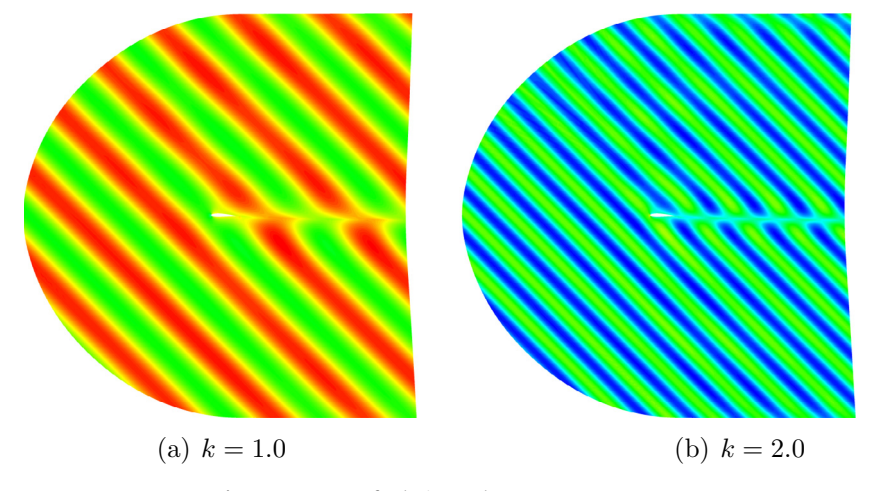


Fig. 13. Contours of velocity v when t = 180, $AOA = 2^{\circ}$.

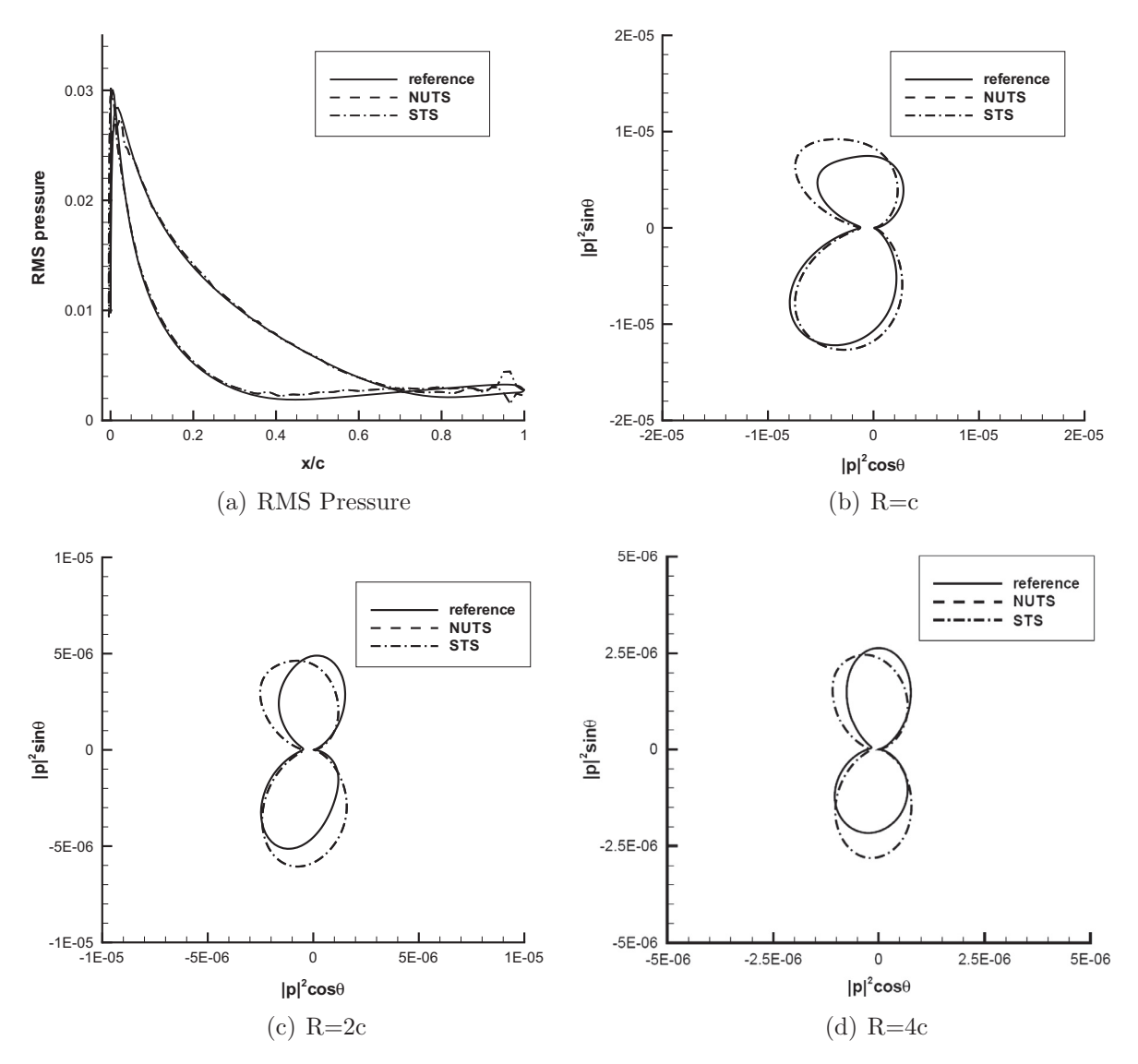


Fig. 14. The RMS pressure on airfoil surface and the acoustic intensity, k = 1.0, $AOA = 0^{\circ}$.

$$\frac{\partial u}{\partial t} + \frac{\partial v}{\partial x} = 0
\frac{\partial v}{\partial t} + \frac{\partial u}{\partial x} = 0, x \in [-50, 50]$$
(10)

and

$$u(x,0) = \exp\left(-\ln 2\left(\frac{x-x_0}{r_0}\right)^2\right), \quad x_0 = 0, \quad r_0 = 6.0$$

$$v(x,0) = 0$$

Eq. (10) is discretized in an overset grid composed of two blocks as indicated in Fig. 5a, of which the left block starts from x=-53 and is partitioned by 57 points with a uniform spacing $\Delta x_1=1.0$, and the right block starts from x=-1.5 and contains 107 points with a uniform spacing $\Delta x_2=0.5$. The last 3 points on both ends of each block are calculated by spatial interpolation, and the dashed lines in Fig. 5 indicate the interface of the blocks. Using the same local CFL condition, the time step sizes in two blocks satisfy a ratio $\Delta t_1:\Delta t_2=2:1$. The 4th-order non-uniform time step LDDRK6 (6 stages) scheme is employed for time integration, while the DRP scheme with high-order interpolation technique is used for spatial discretization. The initial Gaussian shaped pulse is split into two

that move in opposite directions. By applying the periodic boundary condition, the two pulses propagate back and forth repeatedly in the overset grid. Fig. 5b gives the solution at t=625. For comparison, the case is also re-run with a single uniform time step Δt_2 (STS) and shown in Fig. 5b as well. Good agreement is observed.

In order to estimate the computational benefits by the NUTS algorithm over a single uniform time step method, we define a time cost reduction factor *S* as follows

$$S = 1 - \frac{T_m}{T_s} \tag{11}$$

where T_m is the computational time by using the NUTS algorithm, and T_s is the one by using a single uniform time step. Excluding the cost of overset-point coupling for the moment, the ideal factor can be estimated as

$$S = 1 - \frac{T_m}{T_s} = 1 - \frac{\sum_{i=1}^{M} (N_{e,i} / \Delta t_i)}{\left(\sum_{i=1}^{M} N_{e,i}\right) / \Delta t_{min}}$$
(12)

where $N_{e,i}$ denotes the number of the grid points in the i-th block with a local time step size Δt_i , and $\Delta t_{min} = \min_{1 \le i \le M} (\Delta t_i)$ is the

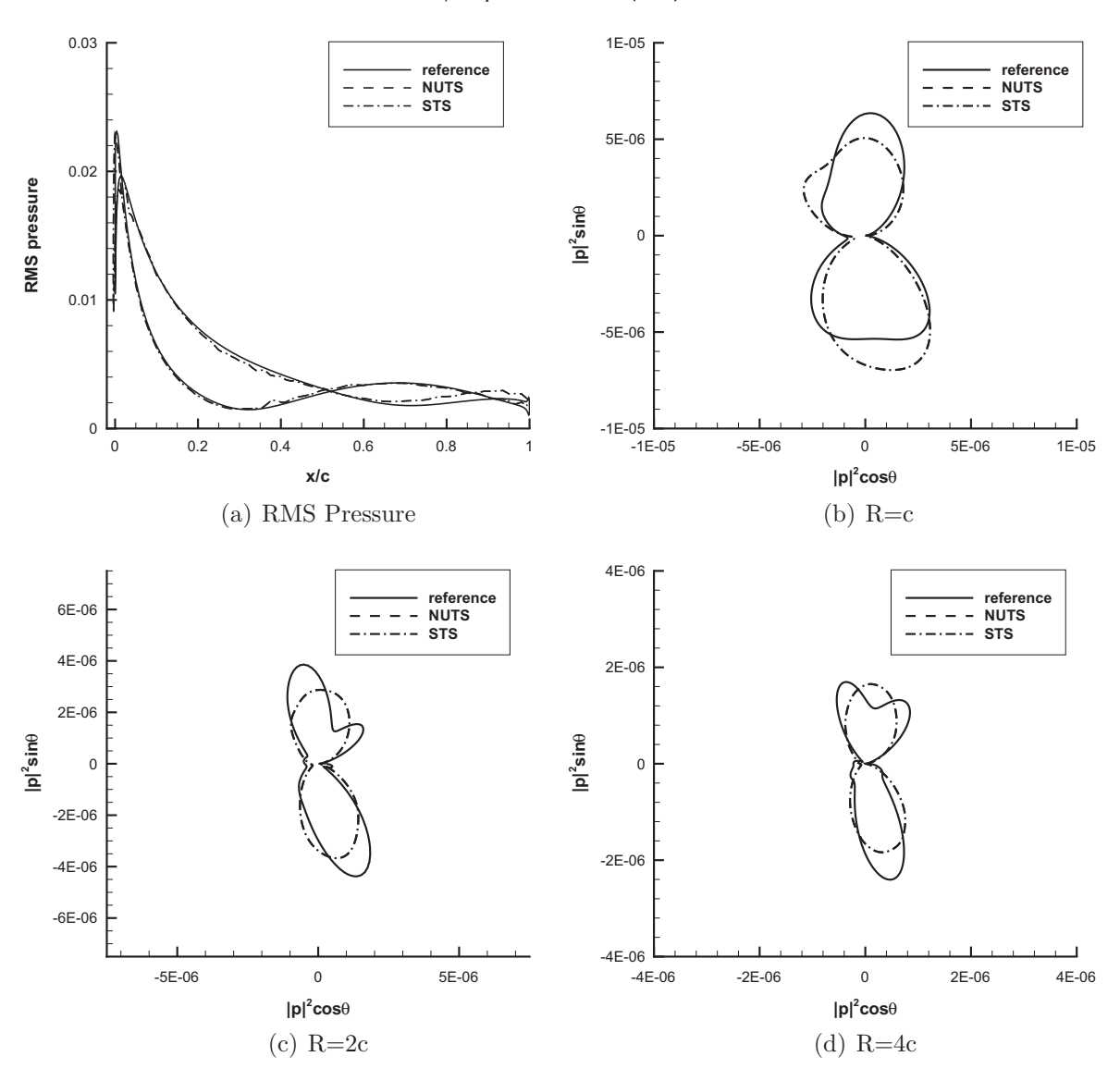


Fig. 15. The RMS pressure on airfoil surface and the acoustic intensity, k=2.0, $AOA=0^{\circ}$.

smallest of all M blocks of grids. The actual reduction factor can be obtained by comparing the actual computational time costs as

$$S^* = 1 - \frac{T_m^*}{T_s^*} \tag{13}$$

where a superscript '*' means the quantity in actual computation. The ideal and the actual cost reduction factors for all the cases studied in this paper are shown in Table 2. For the test presented in this section, the reduction reaches $S^* = 72.4\%$, and is only slightly lower than the ideal estimation S = 73.8%.

4.2. Two dimensional case

4.2.1. Acoustic propagation

A two dimensional acoustic pulse is simulated by solving the linearized Euler equations,

$$\frac{\partial \mathbf{U}}{\partial t} + \frac{\partial \mathbf{E}}{\partial x} + \frac{\partial \mathbf{F}}{\partial y} = \mathbf{0} \tag{14}$$

where

$$\mathbf{U} = \begin{bmatrix} \rho \\ u \\ v \\ p \end{bmatrix}, \quad \mathbf{E} = \begin{bmatrix} M_x \rho + u \\ M_x u + p \\ M_x v \\ M_x p + u \end{bmatrix}, \quad \mathbf{F} = \begin{bmatrix} M_y \rho + v \\ M_y u \\ M_y v + p \\ M_v p + v \end{bmatrix}$$

and $x \in [-100, 100], y \in [-100, 100]$.

In the example, the background flow is uniform with $M_x=0.5$ and $M_y=0$, and a 2D Gaussian pulse is excited at t=0 as

$$p = \exp\left[-\ln 2\left(\frac{x^2 + y^2}{9}\right)\right]$$

$$\rho = \exp\left[-\ln 2\left(\frac{x^2 + y^2}{9}\right)\right] + 0.1 \exp\left[-\ln 2\left(\frac{(x - 67)^2 + y^2}{25}\right)\right]$$

$$u = 0.04y \exp\left[-\ln 2\left(\frac{(x - 67)^2 + y^2}{25}\right)\right]$$

$$v = -0.04(x - 67) \exp\left[-\ln 2\left(\frac{(x - 67)^2 + y^2}{25}\right)\right]$$

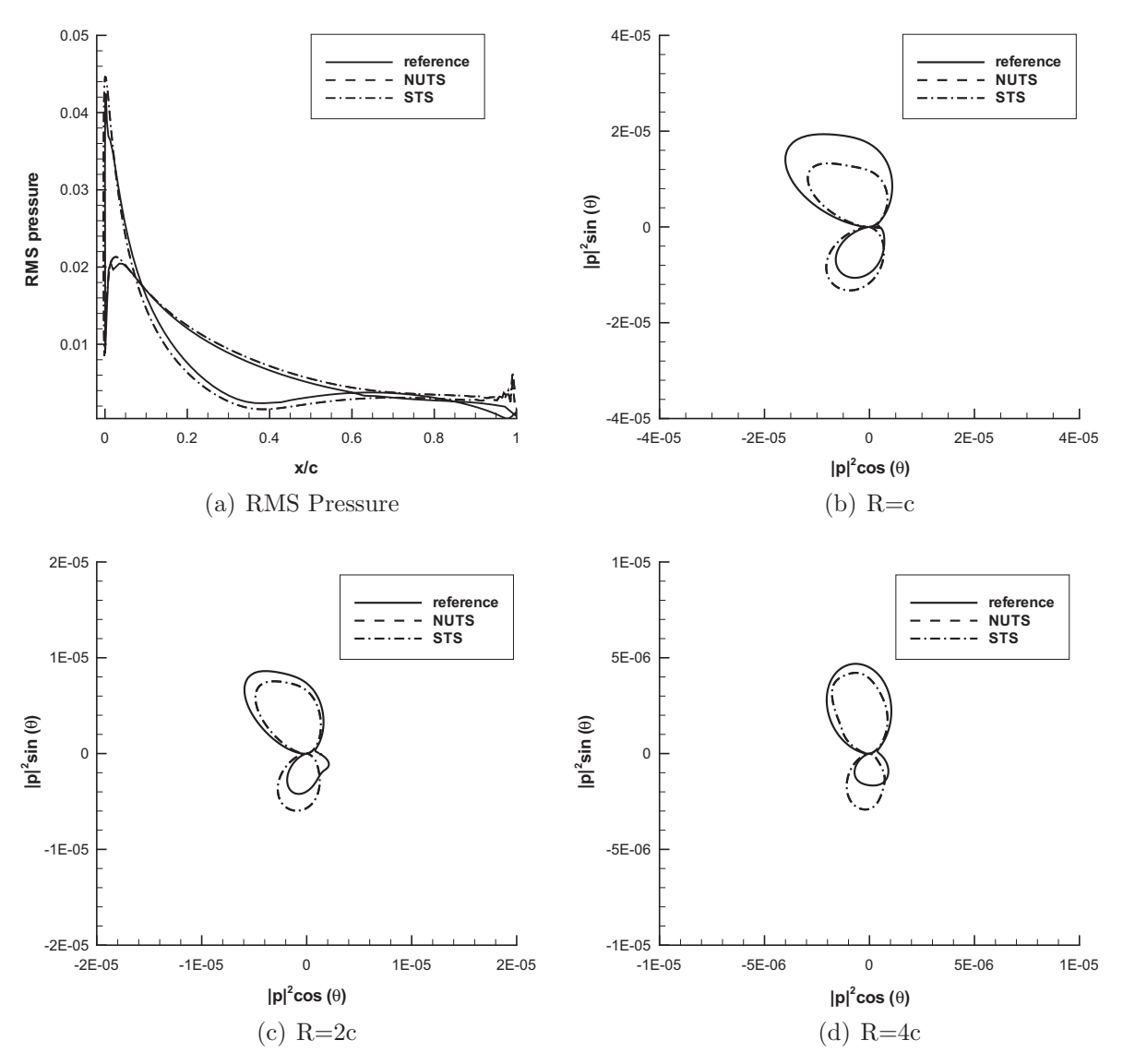


Fig. 16. The RMS pressure on airfoil surface and the acoustic intensity, k = 1.0, $AOA = 2^{\circ}$.

Overset grids are used for this problem, as shown in Fig. 6. It consists of 13 overlapping structured grid blocks, to validate the coupling and stability of the NUTS schemes presented in the previous sections. In Fig. 6, each block is shown with a grid spacing index number. The blocks with the same index number have the same grid spacing, and those spacings satisfy ratios $\Delta_1: \Delta_2: \Delta_3: \Delta_4=1:2:5:16$, where the smallest one is $\Delta_1=0.05$. The total number of grid points under each block index is $N_1=2401, N_2=13,524, N_3=30,084$, and $N_4=65,100$, respectively.

A uniform CFL number is applied throughout the computational domain, resulting in the non-uniform time steps as $\Delta t_1:\Delta t_2:\Delta t_3:\Delta t_4=1:2:5:16$. The numerical results at t=30 and 60 are shown in Fig. 7 for pressure and Fig. 8 for density. For comparison, the calculation has been repeated with a single time step (STS) Δt_1 for all blocks. Fig. 9 presents the exact and the numerical solutions along y=0. Good agreements are observed in those comparisons. By definitions given in (12) and (13), Computational time reduction by NUTS algorithm reaches 75.8% when comparing with the cost by STS algorithm, which is slightly lower than the ideal estimate 82.3%. This implies that the overhead due to the coupling procedures is not significant in this test problem.

4.2.2. Single airfoil gust response

In this example, the non-uniform time step (NUTS) scheme is applied to the gust-airfoil interaction problem which is one of the benchmark problems of the fourth CAA workshop [23] and involves an irregular geometry. The response of a 12% thickness Joukowski airfoil to a 2D harmonic vortical gust is considered, and the upstream velocity distribution is given by

$$\mathbf{U} = U_{\infty} \mathbf{i} + \varepsilon \alpha \cos[\mathbf{k} \cdot (\mathbf{x} - \mathbf{i}U_{\infty}t)] \tag{15}$$

where U_{∞} is the velocity of the free stream, $\mathbf{k}=(k_1,k_2)$ is the corresponding wavenumber vector of the gust, and the amplitude of the vortex disturbance is determined by ε .

Two Joukowski airfoils are considered, of which the first is symmetric and with an angle of attack (AOA) 0° , and the other is of the camber ratio 0.02 and with $AOA = 2^{\circ}$. In both cases, the background flow is calculated by a CFD tool. For small amplitude ϵ , the acoustic field can be described by the linearized Euler equations as follows,

$$\frac{\partial \boldsymbol{U}}{\partial t} + \boldsymbol{A}_x \frac{\partial \boldsymbol{U}}{\partial x} + \boldsymbol{A}_y \frac{\partial \boldsymbol{U}}{\partial y} + (\boldsymbol{B}_x + \boldsymbol{B}_y) \boldsymbol{U} = \boldsymbol{0} \tag{16}$$

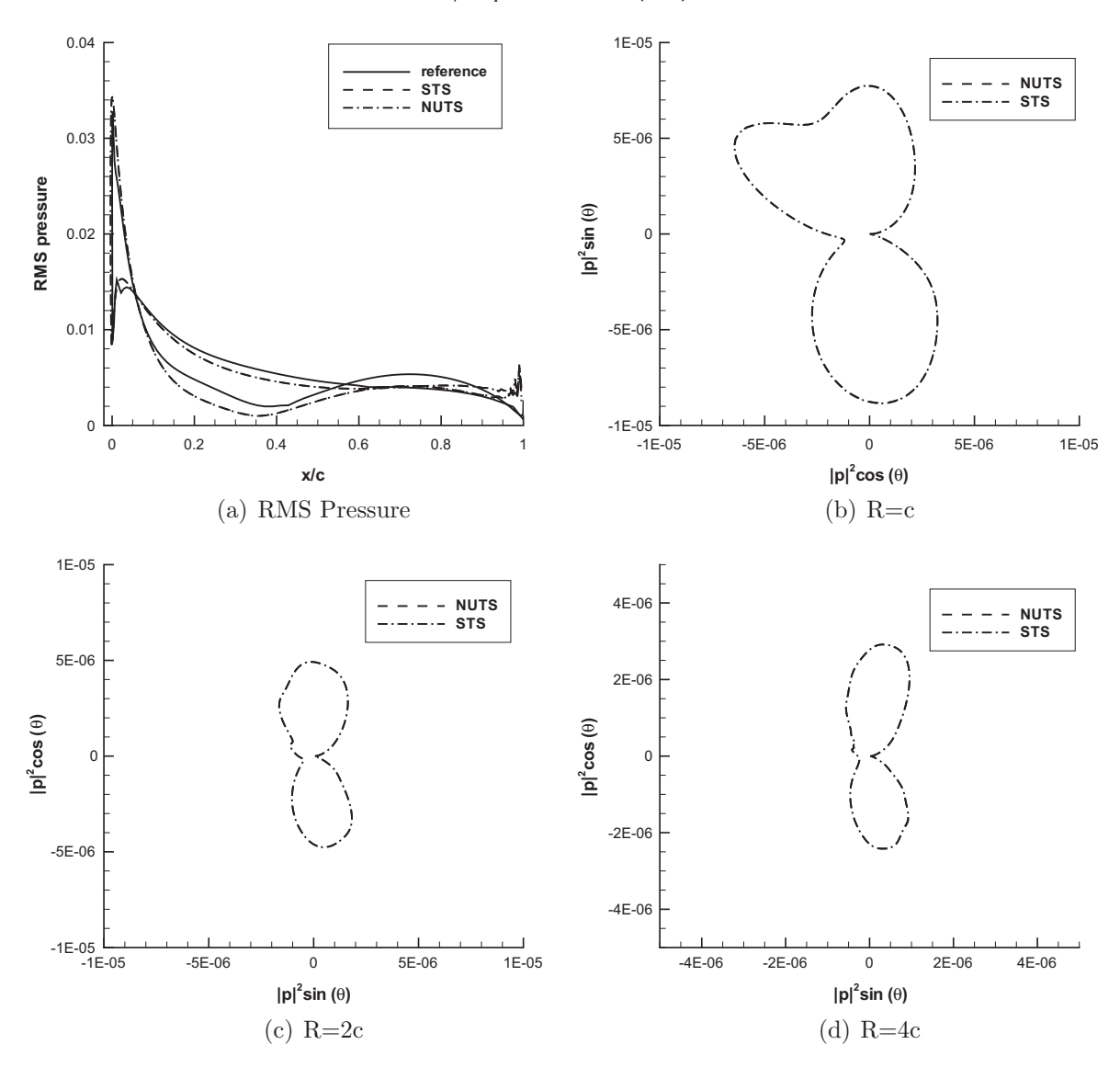


Fig. 17. The RMS pressure on airfoil surface and the acoustic intensity, k=2.0, $AOA=2^{\circ}$.

where

$$\begin{split} \boldsymbol{U} &= \begin{bmatrix} \rho \\ u \\ v \\ p \end{bmatrix}, \ \boldsymbol{A}_x = \begin{bmatrix} \bar{u} & \bar{\rho} & 0 & 0 \\ 0 & \bar{u} & 0 & 1/\bar{\rho} \\ 0 & 0 & \bar{u} & 0 \\ 0 & \gamma\bar{\rho} & 0 & \bar{u} \end{bmatrix}, \ \boldsymbol{A}_y = \begin{bmatrix} \bar{v} & 0 & \bar{\rho} & 0 \\ 0 & \bar{v} & 0 & 0 \\ 0 & 0 & \bar{v} & 1/\bar{\rho} \\ 0 & 0 & \gamma\bar{\rho} & \bar{v} \end{bmatrix}, \\ \boldsymbol{B}_x &= \frac{\partial}{\partial x} \begin{bmatrix} \bar{u} & \bar{\rho} & 0 & 0 \\ 0 & \bar{u} & 0 & 0 \\ 0 & \bar{v} & 0 & 0 \\ 0 & \bar{p} & 0 & \gamma\bar{u} \end{bmatrix}, \ \boldsymbol{B}_y = \frac{\partial}{\partial y} \begin{bmatrix} \bar{v} & 0 & \bar{\rho} & 0 \\ 0 & 0 & \bar{u} & 0 \\ 0 & 0 & \bar{v} & 0 \\ 0 & 0 & \bar{p} & \gamma\bar{v} \end{bmatrix}. \end{split}$$

In the present work, the perturbation variables ρ,u,v,p are nondimensionalized by $\bar{\rho},\bar{a}$ and $\bar{\rho}\bar{a}^2$, respectively. In (15), $\varepsilon=0.01$, $U_\infty=0.5$, and the wave numbers are chosen to be $k_1=k_2=1.0$, and 2.0 in the test.

A body-fitted overset C-grid used for the simulation is shown in Fig. 10, where the finest grids are used in the area close to the airfoil to accurately represent the boundary of the geometry, and the coarser grids are used in the blocks away from the airfoil. The grid consists of 36 blocks, on which different time-step sizes are set in different grid blocks according to their smallest characteristic length. The distribution of the time steps in the 36 blocks is

illustrated in Fig. 11, where the block index denotes the time steps that satisfy $\Delta t_1:\Delta t_2:\Delta t_3:\Delta t_4:\Delta t_5:\Delta t_6:\Delta t_7=1:2:4:6:8:12:16$, and Δt_1 is 0.001. In the case with $AOA=0^\circ$, the grid points with the smallest time-step size form 3.1% of the total number of grid points, 98923. In the case of $AOA=2^\circ$, they form 2.2% of the total number of grid points, 155,991.

In order to demonstrate the computational cost reduction by the present non-uniform time step integration scheme, the tests are conducted with both the non-uniform time step (NUTS) and single time step (STS) RK schemes. Fig. 12 gives the mean pressure distribution on airfoil surface and its comparison with the solution given in Ref. [24]. We note that for the case with $AOA = 2^{\circ}$, the mean pressure on the airfoil surface, which is obtained by solving the nonlinear Euler equation, is slight higher than the reference solution, which was calculated by the potential code FLO36 [24]. The difference between the background field used in the present calculation and the one used for the reference solution in Ref. [24] could affect the acoustic intensity in the near field as reported below.

Fig. 13 shows the contours of the v-velocity component. The solutions appear to be smooth and without artifacts at block interfaces. Figs. 14 and 15 give the RMS pressure distribution on airfoil surface and the scattered acoustic intensity in the near field calculated on a circle of radius R = c, 2c and 4c for the case with

 $AOA = 0^{\circ}$. Here c is the chord length of the airfoil. Comparing with the results by using the single time step method, the results by using NUTS-RK method show good agreements. Similar results for the case with $AOA = 2^{\circ}$ are shown in Figs. 16 and 17. Comparisons with the reference solution of [24] are given wherever available. In all the cases shown, while the results from non-uniform time step (NUTS) and single time step (STS) schemes match very closely, differences with the solution given in Ref. [24] are visible. The deviations are attributed to the differences in the mean flows used in the calculations as mentioned earlier. The computational cost reductions are also investigated and listed in Table 2, in which the computational time is saved by as much as 71% to 74% in actual computation in the current problem.

5. Conclusions

The application of non-uniform time step (NUTS) explicit Runge-Kutta scheme is explored for a typical high order finite difference discretization. The general linear formulation of the coupling procedures are given for the exchange of Runge-Kutta stage values that are necessary for the finite difference discretization used in overset grids. Investigation of the stability property reveals that the coupling procedures maintain the original stability limits of the optimized 4-, 5- and 6-stage LDDRK schemes based on local grid sizes. Numerical tests are performed for one and two dimensional acoustic problems. The results illustrate the stability and feasibility of the non-uniform time step RK integration scheme combined with the DRP scheme. Moreover, the overhead in computational cost due to the coupling procedure is found to be limited. In 2D tests presented in the paper, the computational time reduction by the NUTS algorithm is approximately 75%, which is very encouraging. Further development of the present algorithm in applications to other aeroacoustics problems will be reported in the future.

Acknowledgments

This work is supported by Grants from the 973 Program 2012CB720202 and the NSF-DMS-0810946. The authors also would like to acknowledge the support of the 111 Project B07009 of China.

Appendix A. The derivation of formula (4) and (5)

In this Appendix, we will show more details about the derivation of formula (4) and (5) in Section 2.

For linear cases, the Taylor series expansion of $\{\mathbf{k}_i\}$ at intermediate time levels up to order p can be used. Specifically, for Mesh 1 in Fig. 1 we have

$$\begin{split} \tilde{\mathbf{k}}_{1}|_{t=t_{n}} &= \frac{\partial \mathbf{U}}{\partial t} + \Delta \tau_{2} \frac{\partial^{2} \mathbf{U}}{\partial t^{2}} + \frac{\Delta \tau_{2}^{2}}{2!} \frac{\partial^{3} \mathbf{U}}{\partial t^{3}} + \dots + \frac{\Delta \tau_{2}^{p-1}}{(p-1)!} \frac{\partial^{p} \mathbf{U}}{\partial t^{p}} + O(\Delta \tau_{2}^{p}) \\ \tilde{\mathbf{k}}_{2}|_{t=t_{n}} &= \left(\frac{\partial \mathbf{U}}{\partial t} + c_{22} \Delta t_{1} \frac{\partial^{2} \mathbf{U}}{\partial t^{2}} \right) + \Delta \tau_{2} \left(\frac{\partial^{2} \mathbf{U}}{\partial t^{2}} + c_{22} \Delta t_{1} \frac{\partial^{3} \mathbf{U}}{\partial t^{3}} \right) \\ &+ \frac{\Delta \tau_{2}^{2}}{2!} \left(\frac{\partial^{3} \mathbf{U}}{\partial t^{3}} + c_{22} \Delta t_{1} \frac{\partial^{4} \mathbf{U}}{\partial t^{4}} \right) + \dots + \frac{\Delta \tau_{2}^{p-1}}{(p-1)!} \left(\frac{\partial^{p} \mathbf{U}}{\partial t^{p}} + \frac{\partial^{(p+1)} \mathbf{U}}{\partial t^{(p+1)}} \right) \\ \dots & (17) \\ \tilde{\mathbf{k}}_{p}|_{t=t_{n}} &= \left(\frac{\partial \mathbf{U}}{\partial t} + c_{p2} \Delta t_{1} \frac{\partial^{2} \mathbf{U}}{\partial t^{2}} + \dots + c_{pp} \Delta t_{1}^{p-1} \frac{\partial^{p} \mathbf{U}}{\partial t^{p}} \right) \\ &+ \Delta \tau_{2} \left(\frac{\partial^{2} \mathbf{U}}{\partial t^{2}} + c_{p2} \Delta t_{1} \frac{\partial^{3} \mathbf{U}}{\partial t^{3}} + \dots + c_{pp} \Delta t_{1}^{p-1} \frac{\partial^{(p+1)} \mathbf{U}}{\partial t^{(p+1)}} \right) \\ &+ \dots + \frac{\Delta \tau_{2}^{p-1}}{(p-1)!} \left(\frac{\partial^{p} \mathbf{U}}{\partial t^{p}} + c_{p2} \Delta t_{1} \frac{\partial^{(p+1)} \mathbf{U}}{\partial t^{(p+1)}} + \dots + c_{pp} \Delta t_{1}^{p-1} \frac{\partial^{(2p-1)} \mathbf{U}}{\partial t^{(2p-1)}} \right) \end{split}$$

where c_{ij} are related to the Runge–Kutta coefficients a_{ij} as given in Ref. [19].

The relation between $\{\tilde{\mathbf{k}}_i\}$ and $\left\{\frac{\partial^i \mathbf{u}}{\partial t^i}\right\}$ can be found in matrix form

$$\begin{bmatrix} \tilde{\mathbf{k}}_{1} \\ \tilde{\mathbf{k}}_{2} \\ \vdots \\ \tilde{\mathbf{k}}_{p} \end{bmatrix}_{t=t_{p}} = \mathbf{C} \mathbf{P}_{\Delta t_{1}} \mathbf{B}_{\Delta \tau_{2}} \begin{bmatrix} \frac{\partial \mathbf{U}}{\partial t} \\ \frac{\partial^{2} \mathbf{U}}{\partial t^{2}} \\ \vdots \\ \frac{\partial^{p} \mathbf{U}}{\partial t^{p}} \end{bmatrix}_{t=t_{m-1}} + O(\Delta \tau_{2}^{p})$$

$$(18)$$

where C and $P_{\Delta t_1}$ are in the same form as given in Section 2, and $B_{\Delta \tau_2}$ is an upper-triangular matrix of the form

where b_{ij} are the coefficients of Taylor series expansion given below:

$$b_{ij} = \frac{1}{(j-i)!}$$

By (3), formula (4) in Section 2 can be derived with ease.

For Mesh 2 in Fig. 1, the Taylor series expansion of $\{\mathbf{k}_i\}$ at $t=t_n$ up to order p can be utilized. Thus the relation between $\{\tilde{\mathbf{k}}_i\}_{t=t_m}$ and $\{\mathbf{k}_i\}_{t=t_n}$ can be found as formula (5) in the same way.

References

- [1] Tam CKW, Webb JC. Dispersion-relation-preserving finite difference schemes for computational acoustics. J Comput Phys 1993;107:262–81.
- [2] Lele SK. Compact finite difference schemes with spectral-like resolution. J Comput Phys 1992;103:16–42.
- [3] Lin SY, Chen YS. Comparison of higher resolution Euler schemes for aeroacoustics computations. AIAA J 1995;33:237–45.
- [4] Zhuang M, Chen R. Optimized upwind dispersion-relation-preserving finite difference scheme for computational aeroacoustics. AIAA J 1998;36:2146–8.
- [5] Delfs JW. An overlapped grid technique for high resolution CAA schemes for complex geometries. AIAA Paper 2001-2199; 2001.
- 6] Sherer SE, Scott JN. Development and validation of a high-order overset grid flow solver. AIAA Paper 2002-2733; 2002.
- [7] Sherer SE, Visbal MR. Computational study of acoustic scattering from multiple bodies using a high-order overset grid approach. AIAA Paper 2003-3203; 2003.
- [8] Yin J, Delfs JW. Sound generation from gust-airfoil interaction using CAAchimera method. AIAA Paper 2001-2136; 2001.
- [9] Sherer SE, Scott JN. Comparison of highly accurate interpolation methods. AIAA Paper 2001-0282; 2001.
- [10] Tam CKW, Hu FQ. An optimized multi-dimensional interpolation scheme for computational aeroacoustics applications using overset grids. AIAA Paper 2004-2812; 2004.
- [11] Tam CKW, Kurbatskii KA. A wavenumber based extrapolation and interpolation method for use in conjunction with high-order finite difference schemes. J Comput Phys 2000;157:588–617.
- [12] Allampali V, Hixon R. Implementation of multi-time step Adams-Bashforth time marching scheme for CAA. AIAA Paper 2008-29; 2008.
- [13] Garrec TL, Gloerfelt X, Corre C. Multi-size-mesh multi-time-step algorithm for noise computation around an airfoil in curvilinear meshes. AIAA Paper 2007-3504: 2007.
- [14] Gear C, Wells D. Multirate linear multistep method. BIT 1984;24:484–502.
- [15] Günther M, Kvarno A, Rentrop P. Multirate partitioned Runge-Kutta methods. BIT 2001;41:504-14.
- [16] Lin DK, Jiang M, Li XD. A multi-time-step strategy based on an optimized time interpolation scheme for overset grids. J Comput Acoust 2010;18:1–18.
- [17] Tam CKW, Kurbatskii KA. Multi-size-mesh multi-time-step dispersion-relation-preserving scheme for multiple-scales aeroacoustics problems. Int J Comput Fluid Dyn 2003;17:119–32.
- [18] Savcenco V, Hundsdorfer W, Verwer JG. A multirate time stepping strategy for stiff ordinary differential equations. BIT 2007;47:137–55.
- [19] Liu L, Li XD, Hu FQ. Nonuniform time-step Runge-Kutta discontinuous Galerkin method for computational aeroacoustics. J Comput Phys 2010;229:6874-97.

- [20] Hu FQ, Hussaini MY, Manthey JL. Low-dissipation and low-dispersion Runge–Kutta schemes for computational acoustics. J Comput Phys 1996;124:177–91.
 [21] Stanescu D, Habashi WG. 2N-storage low dissipation and dispersion Runge–Kutta schemes for computational acoustics. J Comput Phys 1998;143:674–81.
 [22] Berland J, Bogey C, Bailly C. Low-dissipation and low-dispersion fourth-order Runge–Kutta algorithm. Comput Fluids 2006;35:1459–63.
- [23] Dahl MD. Fourth computational aeroacoustics (CAA) workshop on benchmark problems. NASA/CP-2004-212954; 2004.
 [24] Scott JR. Single airfoil gust response problem. NASA CP 2004-212954; 2004.